IEEE Access
Multidisciplinary | Rapid Review | Open Access Journal

Received June 3, 2019, accepted July 11, 2019, date of publication July 16, 2019, date of current version August 7, 2019.

Digital Object Identifier 10.1109/ACCESS.2019.2929364

Nonlocal Means Filtering Based Speckle Removal Utilizing the Maximum *a Posteriori* Estimation and the Total Variation Image Prior

ZHENHUA ZHOU[1], EDMUND Y. LAM[2], (Fellow, IEEE), AND CHUL LEE[3], (Member, IEEE)

[1]College of Electronics and Information Engineering, Shenzhen University, Shenzhen 518060, China
[2]Imaging Systems Laboratory, Department of Electrical and Electronic Engineering, The University of Hong Kong, Hong Kong
[3]Department of Multimedia Engineering, Dongguk University, Seoul 04620, South Korea

Corresponding author: Zhenhua Zhou (cityu_zzh2011@163.com)

This work was supported in part by the National Natural Science Foundation of China under Grant 61801130, and in part by the National Research Foundation of Korea under Grant NRF-2019R1A2C4069806.

ABSTRACT In this paper, the problem of image speckle removal is addressed. To alleviate the pepper–salt remainder in the speckled image, we propose to utilize the nonlocal means filtering, where the weighting coefficients are derived based on the maximum *a posteriori* estimation with the total variation image prior. As a result, the objective function of the pixel fitting term plus the total variation regularizer is formulated, and it is solved with the majorization–minimization approach. To avoid the computationally intractable step size selection in the huge-scale gradient-based optimization, we split and solve the variables in the pixel fitting term and regularizer by means of the alternating direction method of multipliers. Performance analysis is performed for the Rayleigh and Gamma distributed signal models. The simulation and experimental results show the superior performance compared with other image despeckling methods in terms of various metrics and visual perception.

INDEX TERMS Nonlocal means filtering, speckle, maximum *a posteriori* estimation, total variation image prior, majorization-minimization approach, alternating direction method of multipliers.

I. INTRODUCTION

Speckle noise affects the coherent imaging systems [1], such as ultrasound imaging (UI) [2], laser speckle imaging (LSI) [3], synthetic aperture radar (SAR) [4], etc. In these systems, the intensity scattered by the areas corresponding to the limited sensor resolution and averaged when sampled by the sensor results in a random granular pattern. Commonly, the speckle noise is modeled as multiplicative. In order to extract information from the acquired image in a statistically efficient way, it is essential to remove such noise as much as possible while recovering the signal features of interest, which is our motivation of the despeckling research.

Satisfactory speckle suppression is expected to possess the following properties:

- speckle reduction in the intensity/amplitude homogeneous areas;
- feature preservation (such as edges and delicate textures);
- spatial resolution preservation.

The associate editor coordinating the review of this manuscript and approving it for publication was Madhu S. Nair.

Recently, there have been proposed several kinds of methods [5]–[14] to track the problem of despeckling, which can be categorized into three aspects: 1) subspace-based thresholding; 2) transform domain coefficient estimation and shrinkage; 3) spatial domain filtering. Reference [5] is a typical article regarding the despeckling with the subspace-based thresholding, which consists of conducting singular value decomposition (SVD) for the speckled image, eliminating the components from the image space corresponding to the minor singular values, and recovering the image from a "cleaner space". However, for the speckle noise such as Rayleigh and Gamma distributed, the assumption of low noise level is not convincingly true, which makes the methods with the subspace-based thresholding not statistically efficient for despeckling. In the last decade, there have been proposed many algorithms for image denoising and despeckling in the transform domain, especially in the wavelet domain [6]–[10]. Basically, this class of methods consist of applying some transform to the image observation, estimating the transform-domain coefficients and designing the strategy to modify or threshold these coefficients,

and restoring the image with the inverse transform. Since most of these methods are only applicable to the additive noise models, the logarithmic transform is usually applied to the speckled images prior to the despeckling. On one hand, vast simulation and experimental results have shown the superiority in the image feature preservation at different scales. On the other hand, the statistical property of the speckle noise is changed due to the nonlinear logarithmic operation. Moreover, the full analysis of the intrascale and interscale correlations of the transform-domain coefficients is sophisticated. The consequent inexact modeling of the image and noise then inevitably affects the performance of the transform-domain despeckling algorithms.

To avoid the disadvantages of the above despeckling methods, it is aimed in this paper to focus on the image despeckling with spatial filtering, which has been widely applied to the image denoising and despeckling, see [11]–[13] for the early work. Recently, a cluster-based filtering framework is proposed in [15], [16] for the speckle reduction in the optical coherence tomography (OCT) images. In this framework, the image pixels are firstly clustered into several regions with similar optical properties. Then, excluding the effect of the pixels from the other clusters, the locally adaptive despeckling is applied to each pixel. These methods [11]–[13], [15], [16] used to conduct adaptive spatial filtering through the examination of the local statistics surrounding each pixel, and to take the pixel comparison for weighting. Nowadays, it is publicly agreed that, these local and pixel-based methods commonly bear two nasty disadvantages, that is 1) heavy dependency on the local window size and orientation; and 2) ambiguity and distortion after filtering due to the limited samples for the local filtering and the instability of weighting from the pixel comparison. To conquer these problems, the idea of nonlocal means filtering based on the patch similarity has been proposed since [14], where the image ''patch'' refers to the pixel block centered at some pixel. The core of nonlocal means filtering is to fit each pixel with the linear or nonlinear average of the nonlocally selected pixels and with the weighting based on their patch comparison. Following [14], precious effort (see [19]–[21], for example) has been paid to extend such nonlocal means filtering to despeckling. Regrettably, these nonlocal means filtering methods are usually dedicated for some specific speckle models, which narrows down their application range. Consequently, when encountering a different speckle model, we will have to pay effort to develop a new scheme for the sake of despeckling. To lower down the cost of such development, it is required to develop a general nonlocal means filtering-based framework of image despeckling, which is applicable to different statistical models.

Furthermore, for the speckled image, due to the multiplicative noise, its variation is much larger than that of the additively corrupted image. As a result, the conventional spatial filtering methods, which are designed to tackle additive noise, act as the weighted average of the selected pixels and have difficulty in the speckle removal. There still remains obvious pepper and salt disturbance in the processed image. To address this issue, it is necessary to include some regularization into the speckle removal, which is expected to bound the variation of the despeckled images while preserving the sharp edges.

To explore the potential capability of the nonlocal means filtering, we try to construct the general image-despeckling framework from the viewpoint of the maximum *a posteriori* (MAP) estimation. Here, the ''general'' means that our methodology of speckle removal is not limited to a specific statistical model of the image speckle. It is known that the MAP rule, that is to maximize the posterior probability density function (PDF), is statistically efficient in the estimation theory [22].

Basically, the posterior PDF of one image is proportional to the product of its likelihood and prior. Due to the statistical independence, to maximize the image likelihood means fitting each pixel to its corresponding observation. This is a kind of single-pixel-sample fitting, and is not statistically efficient. Motivated by this point, we take advantage of the nonlocal means filtering, and select the similar patches in a nonlocal way, to approximate the expectation of the likelihood. Since one image pixel is fitted to more pixel samples, it is expected to improve the statistical efficiency of the pixel fitting.

As for the image prior, we apply the total variation (TV) prior to the original image, which reflects the structure of the piecewise smooth images [23], such as UI, LSI, SAR, well. In fact, the TV image prior is utilized in a wide range of image deblurring and denoising algorithms [23]–[26].

Accordingly, we formulate the image despeckling as an optimization problem consisting of two parts: the pixel fitting term and the TV regularization term. Here, it is proposed to utilize the majorization-minimization (MM) approach [27], [28] and the alternating direction method of multipliers (ADMM) [29], [30] to solve the produced huge-scale nonlinear optimization problem.

To sum up, in this work, we make the novel contributions as follows:

- Proposing a generalized nonlocal means filtering framework to address the problem of image despeckling. In this work, we utilize the MAP estimation with the TV image prior. Consequently, the corresponding problem formulation consists of two parts: the pixel fitting plus the TV regularization. Indeed, the TV regularization has been applied in [31]–[33], etc. to contribute to the despeckling. Nonetheless, in such works, pixel fitting is conducted pixel pairwise and thus, in a local way. Instead, we select the similar patches in a nonlocal way for the pixel fitting. Simulation and experimental results demonstrate the image quality improvement of our despeckling framework.
- Designing the scheme based on the MM approach and the ADMM to solve the resultant huge-scale nonlinear optimization problem of despeckling. To avoid the computationally heavy step size selection in the conventional gradient-based optimization, we firstly relax

this problem as an iterative convex one through the MM approach, and then utilize the ADMM to split the variables in the pixel fitting and regularization terms. The former variables are optimized separately, each with the golden search method; while the latter ones are solved as a least squares (LS) solution to the quadratic optimization problem. Both of these two solutions need no search for the step size.

It is worth addressing that our nonlocal means filtering framework is devised in the image's linear-scale & spatial domain in this paper. Of course, once the image's probabilistic distribution in the logarithmic scale or some transform domain is derived, following the methodology, this framework is still applicable to the different scale or transform domain.

The rest of this paper is organized as follows. By means of the MAP estimation and the nonlocal means filtering, the problem of speckle removal is formulated in Section II. Meanwhile, its solution is provided by utilizing the MM approach and the ADMM. Given the specific examples of the Rayleigh and Gamma distributed signal models, the details of the problem formulation and its solution are illustrated in Section III.A and B. Then, simulation and experimental results are shown in Section III.C and Section IV, respectively, to evaluate the performance of the proposed method by comparing with the state-of-the-art despeckling methods. Finally, the conclusion is drawn in Section V.

II. ALGORITHM DEVELOPMENT

A. PROBLEM FORMULATION

Now consider the observed image, whose intensity at the lexicographically i-th pixel is modeled as

$$z_i = q_i \cdot u_i, \tag{1}$$

for $i = 1, 2, \cdots, N$, where u_i and q_i represent the noiseless part and corrupting speckle noise of the i-th pixel, respectively, and they are assumed statistically independent of each other; N denotes the number of the pixels of the image. Stack z_i, q_i and u_i as the vectors $\mathbf{z}$, $\mathbf{q}$ and $\mathbf{u}$, respectively, and rewrite (1) in the vectorial form as follows:

$$\mathbf{z} = \mathbf{q} \circ \mathbf{u}, \tag{2}$$

where $\circ$ stands for the operator of Hadamard product.

For the image prior $p(\mathbf{u})$, we adopt the TV function, that is

$$p(\mathbf{u}) \propto \exp\left(-\lambda TV(\mathbf{u})\right), \tag{3}$$

where the TV function is defined as

$$TV(\mathbf{u}) \triangleq \sum_{i=1}^{N} \sqrt{(\Delta_i^h \mathbf{u})^2 + (\Delta_i^v \mathbf{u})^2}, \tag{4}$$

with the operators $\Delta_i^h \mathbf{u}$ and $\Delta_i^v \mathbf{u}$ denoting the horizontal and vertical first-order differences at the pixel u_i, respectively. In detail, $\Delta_i^h \mathbf{u} = u_i - u_{h(i)}$ and $\Delta_i^v \mathbf{u} = u_i - u_{v(i)}$, with $u_{h(i)}$ and $u_{v(i)}$ denoting the horizontally and vertically nearest pixels to u_i, respectively.

The objective is to suppress speckle for the image, and to provide a better peak signal-to-noise ratio (PSNR) and visual perception. From the viewpoint of statistical signal processing, the basic idea of spatial-domain image denoising is to find a statistically efficient estimate of each image pixel with the use of its relevant counterparts in this image. To serve this purpose, it is proposed to apply the MAP estimation to the image despeckling, which aims to maximize the posterior PDF of the original image $\mathbf{u}$ given the observation $\mathbf{z}$:

$$\begin{aligned} \hat{\mathbf{u}} &= \arg\max_{\mathbf{u}} p(\mathbf{u} \mid \mathbf{z}) \\ &= \arg\max_{\mathbf{u}} L(\mathbf{u} \mid \mathbf{z}) p(\mathbf{u}), \end{aligned} \tag{5}$$

where $L(\mathbf{u} \mid \mathbf{z}) = p(\mathbf{z} \mid \mathbf{u})$ represents the likelihood of $\mathbf{u}$ given the image observation $\mathbf{z}$. This is equivalent to minimizing the negative logarithm of $p(\mathbf{u} \mid \mathbf{z})$ as follows:

$$\begin{aligned} \hat{\mathbf{u}} &= \arg\min_{\mathbf{u}} -\log p(\mathbf{z} \mid \mathbf{u}) + \lambda TV(\mathbf{u}) \\ &\triangleq \arg\min_{\mathbf{u}} f(\mathbf{u}, \mathbf{z}). \end{aligned} \tag{6}$$

Here, it is assumed that the speckle noise q_i is independent and identically distributed (i.i.d.). As a result, (6) is rewritten as follows:

$$\begin{aligned} f(\mathbf{u}, \mathbf{z}) &= -\sum_{i=1}^{N} \log p(z_i \mid u_i) + \lambda TV(\mathbf{u}) \\ &\triangleq f_1(\mathbf{u}, \mathbf{z}) + \lambda f_2(\mathbf{u}). \end{aligned} \tag{7}$$

It is seen from (7) that the objective function $f(\mathbf{u}, \mathbf{z})$ is composed of two parts, that is, the pixel fitting term $f_1(\mathbf{u}, \mathbf{z})$ and the TV regularization term $f_2(\mathbf{u})$. They are balanced through the penalty parameter λ. For a larger λ, the image is regularized to a larger degree and looks more smooth, and vice versa.

Note that $f_1(\mathbf{u}, \mathbf{z})$ is in fact the negative logarithmic likelihood function (NLLF) of u_i given the sample z_i ($i = 1, 2, \cdots, N$). Consequently, to minimize $f_1(\mathbf{u}, \mathbf{z})$ is equivalent to the maximum likelihood (ML) estimation of $\mathbf{u}$. Thus, $f_1(\mathbf{u}, \mathbf{z})$ is regarded as the pixel fitting term which aims to restore the image of interest to the ML solution. However, $f_1(\mathbf{u}, \mathbf{z})$ is decoupled with respect to the different pairs of (u_i, z_i), which means that $f_1(\mathbf{u}, \mathbf{z})$ fits each u_i only to a single pixel sample z_i. From the viewpoint of estimation theory, such pixel fitting is not statistically efficient due to the small number of (in fact only one) samples involved. To overcome such drawback, it is proposed to take advantage of the idea of the nonlocal means filtering to derive a kind of modified NLLF as the pixel fitting term.

Take the expectation of $-\log p(z_i \mid u_i)$ in $f_1(\mathbf{u}, \mathbf{z})$ over z_i in the following standard form:

$$E\left\{-\log p(z_i \mid u_i)\right\} = -\int_{z_i} \log p(z_i \mid u_i) \cdot p(z_i \mid u_i) dz_i, \tag{8}$$

which is complicated to compute due to the generic form of $p(z_i|u_i)$.

To handle $E\left\{-\log p(z_i \mid u_i)\right\}$ of (8), we need to relax the continuous integration in (8) to a discrete summation.

For each image pixel z_i, we collect the pixel samples $z_{i,j}$ from the whole image $\mathbf{z}$ so that $z_{i,j}$ and z_i are similar enough to be regarded as originating from the same distribution. As a result, (8) is relaxed as follows:

$$E\{-\log p(z_i \mid u_i)\} \approx -\sum_{j=1}^{N_i} \log p(z_{i,j} \mid u_i) \cdot p(z_{i,j} \mid u_i), \quad (9)$$

where N_i is the number of the collected pixel samples $z_{i,j}$ for each image pixel z_i.

It is natural to regard the pixel sample $z_{i,j}$ similar to z_i given a large value of $p(z_{i,j} \mid u_i)$. In the nonlocal means filtering, instead of utilizing $p(z_{i,j} \mid u_i)$ to evaluate the similarity between the pixel samples z_i and $z_{i,j}$, we compare z_i and $z_{i,j}$ with the image patches centered at z_i and $z_{i,j}$ [14], [34]. Since the pixels within one patch are highly correlated and the image patch bears the ability to reflect the structural characteristic of one pixel, the comparison of two patches is expected to be more robust than that of two pixels to measure the similarity between pixels.

Denote $\mathbf{z}_i$ and $\mathbf{z}_{i,j}$ as the image patches, which are vectorized as columns and centered at z_i and $z_{i,j}$, respectively. To utilize the patch similarity, we firstly select the patches $\mathbf{z}_{i,j}$ $(j = 1, 2, \cdots, N_i)$ similar to $\mathbf{z}_i$ from the whole image. Correspondingly, we replace the similarity measure $p(z_{i,j} \mid u_i)$ in (9) with $p(\mathbf{z}_{i,j} \mid \mathbf{u}_i)$. As a result, (9) is modified as

$$E\{-\log p(z_i \mid u_i)\} \approx -\sum_{j=1}^{N_i} \log p(z_{i,j} \mid u_i) \cdot p(\mathbf{z}_{i,j} \mid \mathbf{u}_i) \quad (10)$$

with $\mathbf{u}_i$ denoting the noiseless part of $\mathbf{z}_i$.

Due to the fact that the noiseless patch $\mathbf{u}_i$ is unavailable in practice, it is impossible to acquire the true value of $p(\mathbf{z}_{i,j} \mid \mathbf{u}_i)$. Hence, we adopt the patch similarity measure proposed in [20], denoted by $w_{i,j}$, as a substitute for $p(\mathbf{z}_{i,j} \mid \mathbf{u}_i)$:

$$w_{i,j} = \prod_{k=1}^{L} \left(\frac{s\left(\mathbf{z}_i(k), \mathbf{z}_{i,j}(k)\right)}{c} \right)^{\frac{g_{\sigma,k}}{h}}, \quad (11)$$

with L denoting the number of the pixels of one image patch, and $\mathbf{z}_i(k)$ $(k = 1, 2, \cdots, L)$ being the k-th element of $\mathbf{z}_i$. Here, $s(\mathbf{z}_i(k), \mathbf{z}_{i,j}(k)) = p(\log \mathbf{z}_i(k) - \log \mathbf{z}_{i,j}(k) \mid \mathbf{u}_i(k) = \mathbf{u}_{i,j}(k))$ is the conditional PDF of $\log \mathbf{z}_i(k) - \log \mathbf{z}_{i,j}(k)$ given that the corresponding true values $\mathbf{u}_i(k)$ and $\mathbf{u}_{i,j}(k)$ are equal, and it is scaled by $c = \max_{x,y>0} s(x, y)$. It is proven in [20] that $c = s(z_c, z_c)$ with z_c being a constant larger than zero. In addition, $g_{\sigma,k}$ represents a sampled two-dimensional Gaussian kernel with the mean of zero and the standard deviation of σ, which is defined as

$$g_{\sigma,k} \triangleq \frac{1}{A} \exp\left(-\frac{k_1^2 + k_2^2}{2\sigma^2} \right), \quad (12)$$

with $A = \sum_{k_1,k_2} \exp\left(-\frac{k_1^2+k_2^2}{2\sigma^2} \right)$, and (k_1, k_2) denoting the two-dimensional position of $\mathbf{z}_i(k)$ relative to the center of the image patch $\mathbf{z}_i$; $h > 0$ controls the amount of filtering. The reasonability of the above similarity measure is analyzed and demonstrated in [20]. Accordingly, (10) is rewritten as:

$$E\{-\log p(z_i \mid u_i)\} \approx -\sum_{j=1}^{N_i} w_{i,j} \log p(z_{i,j} \mid u_i). \quad (13)$$

Substitute (13) for each $-\log p(z_i \mid u_i)$ of $f(\mathbf{u}, \mathbf{z})$, (6) becomes

$$\begin{aligned} \hat{\mathbf{u}} &= \arg\min_{\mathbf{u}} f(\mathbf{u}, \mathbf{z}) \\ &= \arg\min_{\mathbf{u}} -\sum_{i=1}^{N}\sum_{j=1}^{N_i} w_{i,j} \log p(z_{i,j} \mid u_i) + \lambda TV(\mathbf{u}). \end{aligned} \quad (14)$$

To facilitate the following illustration, $f_1(\mathbf{u}, \mathbf{z})$ in (7) is redefined accordingly as

$$f_1(\mathbf{u}, \mathbf{z}) = -\sum_{i=1}^{N}\sum_{j=1}^{N_i} w_{i,j} \log p(z_{i,j} \mid u_i). \quad (15)$$

Since the expected NLLF of u_i is relaxed by the summation approximation of (13), $\hat{\mathbf{u}}$ of (14) is indeed derived from a kind of quasi MAP (Q-MAP) estimation.

B. SOLUTION TO THE PROBLEM

It is quite challenging to solve (14) due to its nonlinearity and huge-scale optimization variables. In particular, the optimal step size selection is too computationally exhaustive to make its solution practical. To address such difficulty, we firstly relax (14) as an iterative convex problem through the MM approach; and then solve it within the framework of the ADMM, which consists of the solution to a set of single-variable optimization problems and that to a quadratic optimization problem. As a result, the computationally exhaustive step size selection is avoided. This is our motivation to devise such a solving scheme. The details are described as follows.

1) RELAXING (14) AS AN ITERATIVE CONVEX PROBLEM WITH THE MM APPROACH

In the MM approach, the denoised image $\hat{\mathbf{u}}$ is solved in an iterative way. To begin with, we assume that $f(\mathbf{u}, \mathbf{z})$ of (14) is second-order differentiable for the moment (indeed, this condition is satisfied for the calculation examples in Section III), and define $\mathbf{u}^{(t)}$ as the current image iterate and $Q(\mathbf{u} \mid \mathbf{u}^{(t)})$ as the function majoring $f(\mathbf{u}, \mathbf{z}) = f_1(\mathbf{u}, \mathbf{z}) + \lambda f_2(\mathbf{u})$ of (14):

$$f(\mathbf{u}^{(t)}, \mathbf{z}) = Q(\mathbf{u}^{(t)} \mid \mathbf{u}^{(t)}), \quad (16)$$

$$f(\mathbf{u}, \mathbf{z}) \le Q(\mathbf{u} \mid \mathbf{u}^{(t)}), \quad for\ \mathbf{u} \ne \mathbf{u}^{(t)}. \quad (17)$$

At each iteration, $\mathbf{u}^{(t+1)}$ is obtained according to:

$$\mathbf{u}^{(t+1)} = \arg\min_{\mathbf{u}} Q(\mathbf{u} \mid \mathbf{u}^{(t)}) \quad (18)$$

so that

$$\begin{aligned} f(\mathbf{u}^{(t+1)}, \mathbf{z}) &\le Q(\mathbf{u}^{(t+1)} \mid \mathbf{u}^{(t)}) \\ &\le Q(\mathbf{u}^{(t)} \mid \mathbf{u}^{(t)}) \\ &= f(\mathbf{u}^{(t)}, \mathbf{z}). \end{aligned} \quad (19)$$

Once $f(\mathbf{u}^{(t)}, \mathbf{z})$ converges to $f^* = f(\mathbf{u}^*, \mathbf{z})$ for some stationary point $\mathbf{u}^*$, we take $\mathbf{u}^*$ as $\hat{\mathbf{u}}$ of (14).

It can be seen from (19) that the sequence $f(\mathbf{u}^{(t)}, \mathbf{z})$, $t = 0, 1, \cdots$, or the solution $\mathbf{u}^{(t)}$, is more and more "satisfactory" in terms of $f(\mathbf{u}, \mathbf{z})$. It can be proved that [35], $f(\mathbf{u}^{(t)}, \mathbf{z})$ converges monotonically to $f^* = f(\mathbf{u}^*, \mathbf{z})$ for some stationary point $\mathbf{u}^*$, as long as $Q(\mathbf{u} \mid \mathbf{u}^{(t)})$ is continuous with respect to both $\mathbf{u}$ and $\mathbf{u}^{(t)}$. This means that even if we cannot find the globally optimal solution of (14) from (18), the solution improves gradually through iteration. As a result, $\hat{\mathbf{u}} = \mathbf{u}^*$ gives the expected solution of (14). Conventionally, the loop of the MM approach is stopped after a fixed number of iterations.

It is suggested in [36] that the TV norm in (14) be majored by the quadratic function

$$\tilde{f}_2(\mathbf{u}) = \frac{1}{2}\mathbf{u}^T\mathbf{D}^T\mathbf{R}^{(t)}\mathbf{D}\mathbf{u} + C, \tag{20}$$

with C some constant, $\mathbf{R}^{(t)} = diag\left(\left[\mathbf{r}^{(t)T}\ \mathbf{r}^{(t)T}\right]^T\right)$, $\mathbf{r}^{(t)} = \left[1/\sqrt{(\Delta_i^h\mathbf{u}^{(t)})^2 + (\Delta_i^v\mathbf{u}^{(t)})^2}, i = 1, 2, \cdots, N\right]$, $\mathbf{D} = \left[(\mathbf{D}^h)^T\ (\mathbf{D}^v)^T\right]^T$, $\mathbf{D}^h$ and $\mathbf{D}^v$ being the horizontal and vertical differential operators, respectively. Reference [36] demonstrates that $\tilde{f}_2(\mathbf{u})$ defined in (20) satisfies both the convexity and the conditions of (16) and (17). Accordingly, $Q(\mathbf{u} \mid \mathbf{u}^{(t)})$, which majors $f(\mathbf{u}, \mathbf{z})$ of (14), takes the following form:

$$Q(\mathbf{u} \mid \mathbf{u}^{(t)}) = f_1(\mathbf{u}, \mathbf{z}) + \frac{1}{2}\lambda\mathbf{u}^T\mathbf{D}^T\mathbf{R}^{(t)}\mathbf{D}\mathbf{u} + C. \tag{21}$$

Unfortunately, although we have relaxed the TV norm as the quadratic (but coupled) function, $\frac{1}{2}\mathbf{u}^T\mathbf{D}^T\mathbf{R}^{(t)}\mathbf{D}\mathbf{u} + C$, different from the case in [36] that the pixel fitting term is also quadratic and $\mathbf{u}^{(t)}$ is updated in each iteration as an LS solution, the pixel fitting term (15) in our problem formulation is generally nonlinear, making the overall optimization of (18) coupled and nonlinear. As a result, it is tough to solve (14) although it has been relaxed as an iterative convex problem, due to the fact that for the gradient-based solver, the selection of the optimal step size is always in need [37]. It is desired to find such an "optimal" step size that can bring about the decrease of the objective function as much as possible. However, this work is vastly complex, especially for the huge-scale optimization. To address the above difficulty, the ADMM is adopted.

2) DIVIDING THE PROBLEM OF (18) INTO TWO TRACTABLE SUBPROBLEMS WITH THE ADMM

To solve the problem of (18), we convert $Q(\mathbf{u} \mid \mathbf{u}^{(t)})$ of (21) into the following equivalent form by splitting the variables in $f_1(\cdot)$ and in the remaining part of $Q(\cdot)$ into two separate set, denoted by $\mathbf{u}$ and $\mathbf{v}$, respectively, and imposing the equivalence constraint between them:

$$\begin{aligned} &\mathcal{Q}(\mathbf{u}, \mathbf{v} \mid \mathbf{u}^{(t)}) = f_1(\mathbf{u}, \mathbf{z}) + \lambda/2 \cdot \mathbf{v}^T\mathbf{D}^T\mathbf{R}^{(t)}\mathbf{D}\mathbf{v}, \\ &subject\ to:\ \mathbf{u} = \mathbf{v}. \end{aligned} \tag{22}$$

Then, the ADMM is utilized to search for the optimal solution of (22) iteratively [30], [38]:

$$\begin{aligned} \mathbf{u}_{(k+1)} &= \arg\min_{\mathbf{u}} \mathcal{Q}(\mathbf{u}, \mathbf{v}_{(k)} \mid \mathbf{u}^{(t)}) \\ &\quad + \mu/2 \cdot \|\mathbf{u} - \mathbf{v}_{(k)} - \boldsymbol{\delta}_{(k)}\|_2^2, \end{aligned} \tag{23}$$

$$\begin{aligned} \mathbf{v}_{(k+1)} &= \arg\min_{\mathbf{v}} \mathcal{Q}(\mathbf{u}_{(k+1)}, \mathbf{v} \mid \mathbf{u}^{(t)}) \\ &\quad + \mu/2 \cdot \|\mathbf{u}_{(k+1)} - \mathbf{v} - \boldsymbol{\delta}_{(k)}\|_2^2, \end{aligned} \tag{24}$$

$$\boldsymbol{\delta}_{(k+1)} = \boldsymbol{\delta}_{(k)} - (\mathbf{u}_{(k+1)} - \mathbf{v}_{(k+1)}), \tag{25}$$

with μ being a user parameter trading off the convergence and converging speed. Normally, a large value of μ enhances the possibility of the ADMM's convergence, while a smaller one speeds up the algorithm. After each iteration of the ADMM, the solution is expected to approach that to (18) more closely. The convergent solution of the ADMM is taken as $\mathbf{u}^{(t+1)}$ of (18).

Up to now, the optimization problem of (18) is converted to two separate subproblems of (23) and (24), which are related through (25). As a result, we need to solve $\mathbf{u}_{(k+1)}$ and $\mathbf{v}_{(k+1)}$ instead.

Here, $\mathbf{u}_{(k+1)}$ and $\mathbf{v}_{(k+1)}$ are solved in a separate way, and they are related through the intermediate variables $\boldsymbol{\delta}_{(k+1)}$ and $\boldsymbol{\delta}_{(k)}$ as in (25). Referring to the analytical form of $f_1(\mathbf{u}, \mathbf{z})$ (15), it is seen that solving $\mathbf{u}_{(k+1)}$ is decoupled with respect to u_i ($i = 1, 2, \cdots, N$). Therefore, the elements of $\mathbf{u}_{(k+1)}$ are able to be solved with a one-dimensional search method separately. As for $\mathbf{v}_{(k+1)}$, it is obtained as an LS solution to a quadratic optimization problem. As a result, in the whole procedure of the ADMM, there is no need of the search for the optimal step size. This point explains the motivation of the work of this subsection.

To sum up, the steps of the whole solution procedure for $\hat{\mathbf{u}}$ of (14) is listed in Algorithm 1. The ADMM approach illustrated above, which aims to solve $\mathbf{u}^{(t+1)}$ of (18), is injected

Algorithm 1 Estimating $\hat{\mathbf{u}}$ of (14) With the MM Approach and ADMM

Initialization: $\mu > 0$, $\mathbf{u}^{(0)} = \mathbf{z}$;
for $t = 0, 1, \cdots, 99$ **do**
  (Outer iteration of the MM approach)
  Set $k = 0$ and $\mathbf{u}_{(0)} = \mathbf{v}_{(0)} = \mathbf{u}^{(t)}$
  Solve (23) - (25):
  repeat
    (Inner iteration of the ADMM)
    $\mathbf{u}_{(k+1)} = \arg\min_{\mathbf{u}} f_1(\mathbf{u}, \mathbf{z}) + \mu/2 \cdot \|\mathbf{u} - \mathbf{v}_{(k)} - \boldsymbol{\delta}_{(k)}\|_2^2$;
    $\mathbf{v}_{(k+1)} = \arg\min_{\mathbf{v}} \lambda/2 \cdot \mathbf{v}^T\mathbf{D}^T\mathbf{R}^{(t)}\mathbf{D}\mathbf{v} + \mu/2 \cdot \|\mathbf{u}_{(k+1)} - \mathbf{v} - \boldsymbol{\delta}_{(k)}\|_2^2$;
    $\boldsymbol{\delta}_{(k+1)} = \boldsymbol{\delta}_{(k)} - (\mathbf{u}_{(k+1)} - \mathbf{v}_{(k+1)})$;
    $k = k + 1$;
  until $max\left\{\frac{\|\mathbf{u}_{(k+1)} - \mathbf{u}_{(k)}\|_2}{\|\mathbf{u}_{(k)}\|_2}, \frac{\|\mathbf{v}_{(k+1)} - \mathbf{v}_{(k)}\|_2}{\|\mathbf{v}_{(k)}\|_2}\right\} \leq 10^{-3}$
  $\mathbf{u}^{(t+1)} = \mathbf{u}_{(k)}$
end for
return $\hat{\mathbf{u}} = \mathbf{u}^{(100)}$.

into the outer loop of the MM. Here, the iteration number of the MM approach is set as 100; the loop of the ADMM is stopped when the relative difference between iterations, $\xi = max\left\{\|\mathbf{u}_{(k+1)}-\mathbf{u}_{(k)}\|_2/\|\mathbf{u}_{(k)}\|_2,\ \|\mathbf{v}_{(k+1)}-\mathbf{v}_{(k)}\|_2/\|\mathbf{v}_{(k)}\|_2\right\}$, is not larger than 10^{-3}.

The convergence of the ADMM optimization (23) - (25) to the optimal solution of (18) is provided by the following theorem.

Theorem 1: Suppose that the objective function of (18) is closed and properly convex. Consider the ADMM optimization with arbitrary $\mu > 0$, $\mathbf{v}_{(0)} \in \mathbb{R}^N$ and $\boldsymbol{\delta}_{(0)} \in \mathbb{R}^N$. Let $\{\eta_k \geq 0,\ k = 0, 1, \cdots\}$ and $\{\nu_k \geq 0,\ k = 0, 1, \cdots\}$ be two sequences such that:

$$\sum_{k=0}^{\infty} \eta_k < \infty, \quad \sum_{k=0}^{\infty} \nu_k < \infty. \tag{26}$$

Suppose that the three sequences $\left\{\mathbf{u}_{(k)} \in \mathbb{R}^N,\ k = 0, 1, \cdots\right\}$, $\left\{\mathbf{v}_{(k)} \in \mathbb{R}^N,\ k = 0, 1, \cdots\right\}$ and $\left\{\boldsymbol{\delta}_{(k)} \in \mathbb{R}^N,\ k = 0, 1, \cdots\right\}$ from (23) - (25) of the ADMM satisfy that,

$$\eta_k \geq \left\|\mathbf{u}_{(k+1)} - \arg\min_{\mathbf{u}} \left\{f_1(\mathbf{u}, \mathbf{z}) + \frac{\mu}{2}\left\|\mathbf{u} - \mathbf{v}_{(k)} - \boldsymbol{\delta}_{(k)}\right\|_2^2\right\}\right\|, \tag{27}$$

$$\nu_k \geq \left\|\mathbf{v}_{(k+1)} - \arg\min_{\mathbf{v}} \left\{\frac{\lambda}{2}\mathbf{v}^T\mathbf{D}^T\mathbf{R}^{(t)}\mathbf{D}\mathbf{v} + \frac{\mu}{2}\left\|\mathbf{u}_{(k+1)} - \mathbf{v} - \boldsymbol{\delta}_{(k)}\right\|_2^2\right\}\right\|, \tag{28}$$

$$\boldsymbol{\delta}_{(k+1)} = \boldsymbol{\delta}_{(k)} - \left(\mathbf{u}_{(k+1)} - \mathbf{v}_{(k+1)}\right). \tag{29}$$

Then, if (18) has a solution denoted by $\mathbf{u}^*$, the sequence $\left\{\mathbf{u}_{(k)}\right\}$ converges as $\mathbf{u}_{(k)} \to \mathbf{u}^*$. If (18) does not have a solution, then at least one of the sequences $\left\{\mathbf{v}_{(k)}\right\}$ and $\left\{\boldsymbol{\delta}_{(k)}\right\}$ diverge.

Proof: See [30].

It is seen from Theorem 1 that, as long as the errors of the sequences $\mathbf{u}_{(k+1)}$ and $\mathbf{v}_{(k+1)}$ are absolutely summable, and the optimization problem is convex, the ADMM will converge to the global solution. Note that it is not necessary to find exactly the optimal solution to $\mathbf{u}_{(k+1)}$ and $\mathbf{v}_{(k+1)}$ in each inner iteration of the ADMM.

III. CALCULATION EXAMPLES AND SIMULATION RESULTS

To clarify the developed image despeckling methodology, here we give the implementation for two specific cases of speckle corrupted image, that is, the Rayleigh [39] and Gamma [4] distributed signal models, which have found much application in ultrasonic [40]–[42], OCT [43], [44] and SAR [45], [46] imaging. Afterwards, we evaluate the performance of the image despeckling with extensive simulation results.

A. RAYLEIGH DISTRIBUTED SIGNAL MODEL

Given the assumption of the Rayleigh distributed speckle noise, the intensity of the observed image, z_i, is modeled with the PDF conditional on u_i as follows:

$$p(z_i|u_i) = \frac{z_i}{\theta^2 u_i^2} \cdot \exp\left(-\frac{z_i^2}{2\theta^2 u_i^2}\right), \quad for\ z_i \geq 0. \tag{30}$$

Here, $\theta > 0$ is the shape parameter of the Rayleigh distribution.

Taking the negative logarithm of (30), neglecting the constant terms, it is derived that for the Rayleigh distributed signal model,

$$f_1(\mathbf{u}, \mathbf{z}) = \sum_{i=1}^{N}\sum_{j=1}^{N_i} w_{i,j}\left(\frac{z_{i,j}^2}{2\theta^2 u_i^2} + 2\log u_i\right). \tag{31}$$

As for $w_{i,j}$, according to its definition (11), we can derive its detail as [20]:

$$w_{i,j} = \prod_{k=1}^{L}\left(\frac{2\mathbf{z}_i(k)\cdot\mathbf{z}_{i,j}(k)}{\mathbf{z}_i^2(k) + \mathbf{z}_{i,j}^2(k)}\right)^{\frac{2g_{\sigma,k}}{h}}. \tag{32}$$

B. GAMMA DISTRIBUTED SIGNAL MODEL

Under the assumption of the Gamma distributed speckle noise, the intensity of the observed image, z_i, is modeled as follows:

$$p(z_i|u_i) = \frac{P^P z_i^{P-1}}{\Gamma(P) u_i^P} \cdot \exp\left(-\frac{Pz_i}{u_i}\right), \quad for\ \ z_i \geq 0, \tag{33}$$

with $\Gamma(\cdot)$ denoting the Gamma function. Here, the shape and rate parameters of the Gamma distribution, α and β, are both equal to $P \geq 1$.

Taking the negative logarithm of (33), neglecting the constant terms, it is derived that for the Gamma distributed signal model,

$$f_1(\mathbf{u}, \mathbf{z}) = \sum_{i=1}^{N}\sum_{j=1}^{N_i} w_{i,j}\left(\frac{Pz_{i,j}}{u_i} + P\log u_i\right). \tag{34}$$

Accordingly, $w_{i,j}$ is derived as [20]:

$$w_{i,j} = \prod_{k=1}^{L}\left(\frac{4\mathbf{z}_i(k)\cdot\mathbf{z}_{i,j}(k)}{\left(\mathbf{z}_i(k) + \mathbf{z}_{i,j}(k)\right)^2}\right)^{\frac{Pg_{\sigma,k}}{h}}. \tag{35}$$

To obtain the global solution of $\mathbf{u}_{(k+1)}$ in Algorithm 1, we find all the knee points of the cost function $f_1(\mathbf{u}, \mathbf{z}) + \mu/2 \cdot \|\mathbf{u} - \mathbf{v}_{(k)} - \boldsymbol{\delta}_{(k)}\|_2^2$, divide its definition region into single-peak parts, find the corresponding minimum points respectively with the golden search method [37], and finally determine $\mathbf{u}_{(k+1)}$ from these minimum points.

C. SIMULATION RESULTS

In this part, we evaluate the performance of the proposed image despeckling methodology through simulation with the "Lena", "House", "Peppers", and "Shepp-Logan" phantom adopted as the testing images and shown in Fig. 1. Here, the "Shepp-Logan" phantom was created by Shepp and Logan [47], and serves as the model of a human

(a) (b) (c) (d)

FIGURE 1. Original images for testing: (a) Lena, (b) House, (c) Peppers, (d) "Shepp-Logan" phantom.

TABLE 1. PSNR performance comparison for Rayleigh distributed speckle.

Input Image	θ	Input PSNR (dB)	Output PSNR (dB)			
			NLF [19]	NLF [20]	S-P F&R	Proposed
Lena	0.5	11.70	21.98	21.97	12.73	23.16
	1.0	8.67	21.91	21.91	16.57	23.15
	1.5	3.20	22.00	22.03	6.96	23.33
House	0.5	10.73	22.10	21.87	12.23	23.46
	1.0	7.75	22.00	21.87	16.27	23.57
	1.5	2.23	22.03	21.85	5.96	23.62
Peppers	0.5	11.98	22.07	22.25	12.54	23.17
	1.0	8.96	22.11	22.26	16.69	23.26
	1.5	3.47	22.10	22.25	7.34	23.25
Shepp-Logan Phantom	0.5	18.26	22.59	27.26	16.21	28.33
	1.0	15.29	22.67	27.21	21.74	28.46
	1.5	9.72	22.55	26.97	15.90	28.29

head in the development and testing of image reconstruction algorithms. The size of these images are set as 256×256.

Here, the quality improvement of the image despeckling is evaluated in terms of the PSNR: $PSNR = 10\log_{10}(255^2 / \|\tilde{\mathbf{u}} - \mathbf{u}\|_2^2)$[1]. By comparison, the nonlocal filtering (NLF) methods [19] and [20] are extended to the simulation scenarios here, and their corresponding results are provided. To address the necessity of nonlocal means filtering in the image despeckling, the results of the single-pixel-sample fitting are also included for comparison, where the following optimization function is used:

$$f(\mathbf{u}, \mathbf{z}) = \|\mathbf{u} - \mathbf{z}\|_2^2 + \lambda TV(\mathbf{u}). \tag{36}$$

This scheme is termed as the single-point fitting and regularization (S-P F&R) method here. Similar problem formulation can also be found in [36], [48], etc., when the system response matrix is taken as identity. For the sake of fairness, the image observation, that is $\mathbf{z}$ of (2), is adopted as the initial value for both of the proposed and S-P F&R methods.

[1]Here, the pixel values are double-precision floating point number ranged in [0, 1].

In addition, for the nonlocal means filtering part of all the above methods, the patch size is set as 3×3. The parameters of the Gaussian kernel in the weighting of (11) are set as $\sigma = 2.5$, $h = 1$ for [20] and the proposed method, which are found empirically to result in good performance.

1) RAYLEIGH DISTRIBUTED SPECKLE

Firstly, we conduct the denoising for the images corrupted by the Rayleigh distributed speckle. The speckle's shape parameter is set as $\theta = 0.5$, 1 and 1.5, respectively.

For the proposed method, the regularization parameter λ is adjusted increasingly, while keeping μ large and guaranteeing the ADMM's convergence. A λ of 10^2 is found to provide the proper tradeoff between the pixel fitting and regularization. Then, μ is tuned decreasingly, and the value of $\mu = 10^4$ is fixed to speed up the ADMM's convergence to within 100 iterations. For the S-P F&R method, λ and μ are tuned as 10 and 10^3, respectively, which are found to provide relatively good overall performance.

Table 1 lists the output PSNRs of the denoised images by the proposed method, the NLF methods [19], [20], the S-P F&R method together with the input PSNR

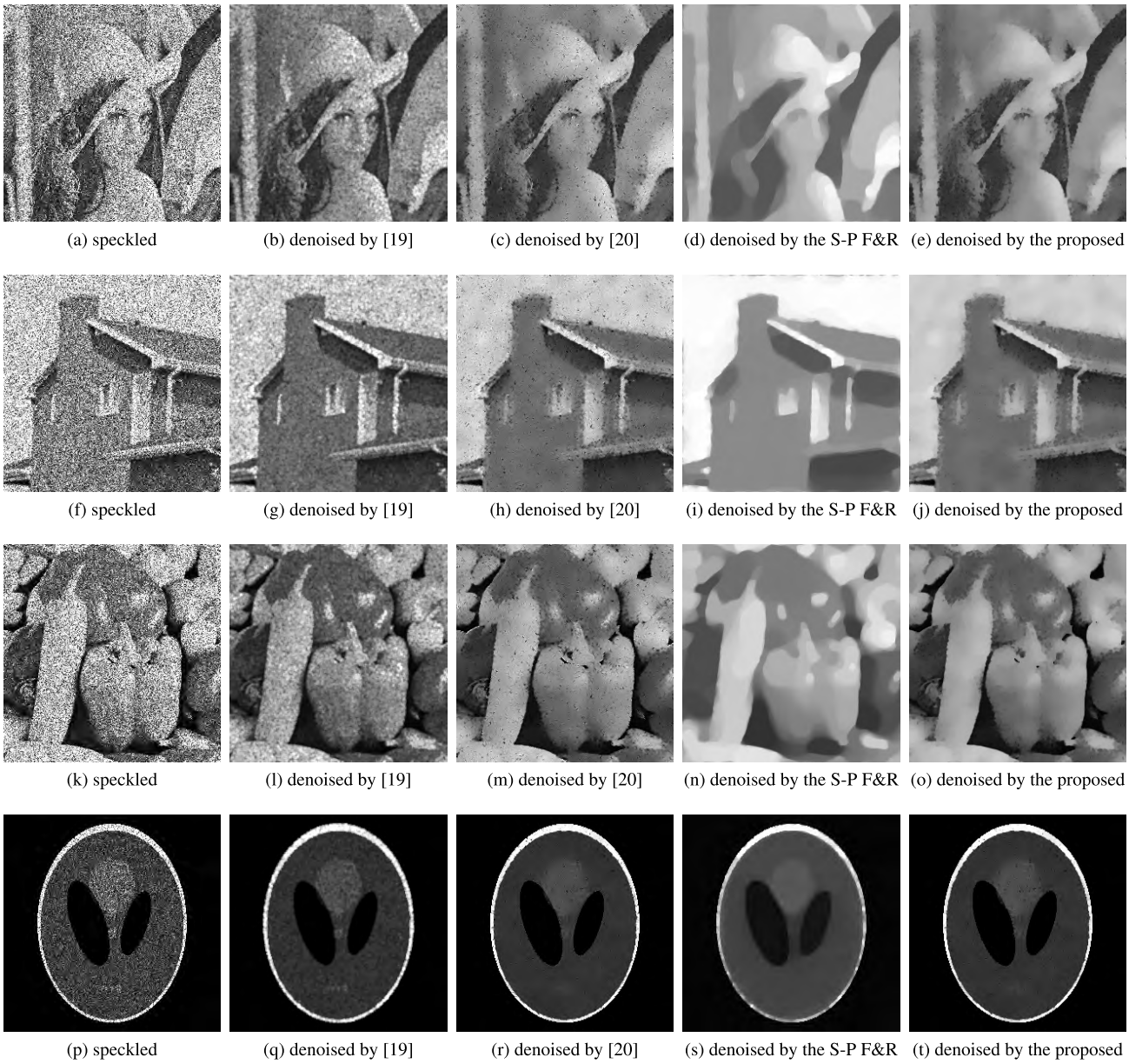

FIGURE 2. Speckled and denoised images for the Rayleigh distributed signal model ($\theta = 1$): (a)-(e): Lena, (f)-(j): House, (k)-(o): Peppers, and (p)-(t): "Shepp-Logan" phantom.

for $\theta = 0.5$, 1, 1.5, and the different testing images. It is seen that the proposed method provides more than 0.92 *dB* PSNR gain compared with the other methods in all the cases; and in most cases, the PSNR gain is above 1.2 *dB*. Note that the proposed method together with the NLF methods [19], [20] always provide similar output PSNRs for the different shape parameters. By comparison, the output PSNR of the S-P F&R method varies much more for the different shape parameters. Especially, although the input PSNR when $\theta = 0.5$ is higher than that when $\theta = 1$, the output PSNR of the S-P F&R method when $\theta = 0.5$ is even lower than that when $\theta = 1$ for all the testing images. This is because the S-P F&R method is unable to utilize the information of the shape parameter during the image despeckling according to (36).

Fig. 2 shows the speckled images and those denoised by the different methods when $\theta = 1$. It is seen that the low PSNR of the S-P F&R method shown in Table 1 is due to its oversmoothing the speckled images. Visually, the proposed method provides more faithful results with less and weaker pepper-salt remainder, which accords with our expectation. For the Shepp-Logan phantom, the main boundaries and the small circle in the center are well preserved.

2) GAMMA DISTRIBUTED SPECKLE

Secondly, we conduct the denoising for the images corrupted by the Gamma distributed speckle. Here, the value of P of the Gamma distribution is set as $P = 4$ and 25, respectively.

TABLE 2. PSNR performance comparison for Gamma distributed speckle.

Input Image	P	Input PSNR (dB)	Output PSNR (dB)			
			NLF [19]	NLF [20]	S-P F&R	Proposed
Lena	4	11.66	22.17	22.77	16.84	23.91
	25	19.62	26.81	28.11	26.79	28.33
House	4	10.68	22.41	22.76	15.27	24.43
	25	18.66	29.70	29.56	27.47	29.88
Peppers	4	11.94	22.41	23.02	17.09	23.97
	25	19.91	26.82	28.04	27.26	28.36
Shepp-Logan Phantom	4	18.08	23.11	27.44	22.14	29.54
	25	26.02	24.35	35.32	31.43	37.63

For the proposed method, the regularization parameter λ is adjusted to 10 to provide the proper tradeoff between the pixel fitting and regularization. Then, μ is tuned as 10^3. For the S-P F&R method, λ is tuned as 10. Accordingly, μ is set as 10^4.

Table 2 lists the output PSNRs of the denoised images together with the input PSNR for $P = 4$, 25, and the different testing images. It is seen that for $P = 4$, the proposed method provides more than 0.95 *dB* PSNR gain compared with the other methods in all the cases; and in most cases, the PSNR gain is above 1.6 *dB*. For $P = 25$ and for the testing images "Lena", "House" and "Peppers", the PSNR advantage of the proposed method over the NLF method [20] is below 0.32 *dB*, which is due to the weak speckle effect.

Fig. 3 shows the speckled images and those denoised by the different methods when $P = 4$. It is seen that there remains obviously more pepper-salt fluctuation in the denoised images by the NLF method [19] and the S-P F&R method. Compared with the NLF method [20], the proposed method still provides more faithful results with less and weaker pepper-salt remainder. It is seen that for the Shepp-Logan phantom, the main boundaries and the small circles in the center and bottom are well preserved.

The above simulation results for the different speckle models and testing images demonstrate that the proposed method with a moderate regularization is advantageous to the image enhancement.

For our solution to the image despeckling, it takes about 3.63 seconds for each inner iteration of the ADMM on a PC with an Intel(R) Core(TM) i7-8750H CPU @ 2.20 GHz, with 16.0 GB of installed memory. The code is, however, not optimized.

Considering the 100 times of outer iterations and the multiple inner iterations in one outer iteration, it appears that the proposed method is quite time-consuming. By comparison, for the Rayleigh distributed speckle, the whole CPU time of the NLF methods [19] and [20] is around 287.10 *s* and 95.11 *s*, respectively. Although the proposed method is not advantageous in running time, it is worth addressing that in order to avoid the computationally heavy step size selection in the gradient-based optimization, the solving scheme of our problem formulation of (14) needs to be designed carefully. In each outer iteration of our solution, the problem (18) is divided into two subproblems (see (23) - (25) and Algorithm 1) by the ADMM, which are both solved with no need to select the step size. As a result, our method is computationally affordable. Otherwise, it is computationally intractable to deal with huge-scale nonlinear optimization.

IV. EXPERIMENTAL RESULTS ON REAL DATA

Now the performance evaluation is conducted for the real OCT image of the porcine carotid arterial wall, obtained using a commercial Lightlab C7-XR Fourier Domain OCT system (Lightlab Imaging). The details of animal imaging protocol have been previously described elsewhere [49]. All the animal procedures were approved by St. Michael's Hospital (Toronto, Ontatio) Animal Care Committee.

Prior to the application of our method to the real data, the intensity of the speckles in the OCT image is modeled as Rayleigh distributed according to [43] and [44]. Thus, it is necessary to estimate the shape parameter θ at first. In [49], the so-called speckle region is taken for the speckle modeling. Since the pixel value of its clean part is varying with respect to the location, such modeling is not accurate. Different from [49], here we make use of the square error (SE) between the observed image, $\mathbf{z}$, and the denoised one from the NLF method [20] with the shape parameter $\tilde{\theta}$, denoted by $\hat{\mathbf{u}}_{NLF}(\tilde{\theta})$, as the criterion for the θ selection. In detail, we divide the preset range of θ, $[0.5\ \ 1.5]$, into several discrete points, select the point where the SE takes the minimum as the estimate of θ, and denote it by $\hat{\theta}$:

$$\begin{aligned}\hat{\theta} &= \arg\min_{\tilde{\theta}} SE(\tilde{\theta}) \\ &= \arg\min_{\tilde{\theta}} 10\log_{10}\left\|\hat{\mathbf{u}}_{NLF}(\tilde{\theta}) - \mathbf{z}\right\|_2^2. \end{aligned} \tag{37}$$

The reasonability of such model parameter selection is originated from the Gaussianity of the estimation error, and its variance estimation (see [22]). The SE calculation results are listed in Table 3. From this table, $\hat{\theta}$ is taken as 0.7.

For medical images, the ability to discern useful details is critical but hard to evaluate. To quantitatively evaluate the performance of the proposed method in comparison with that of the other methods, several metrics are calculated for

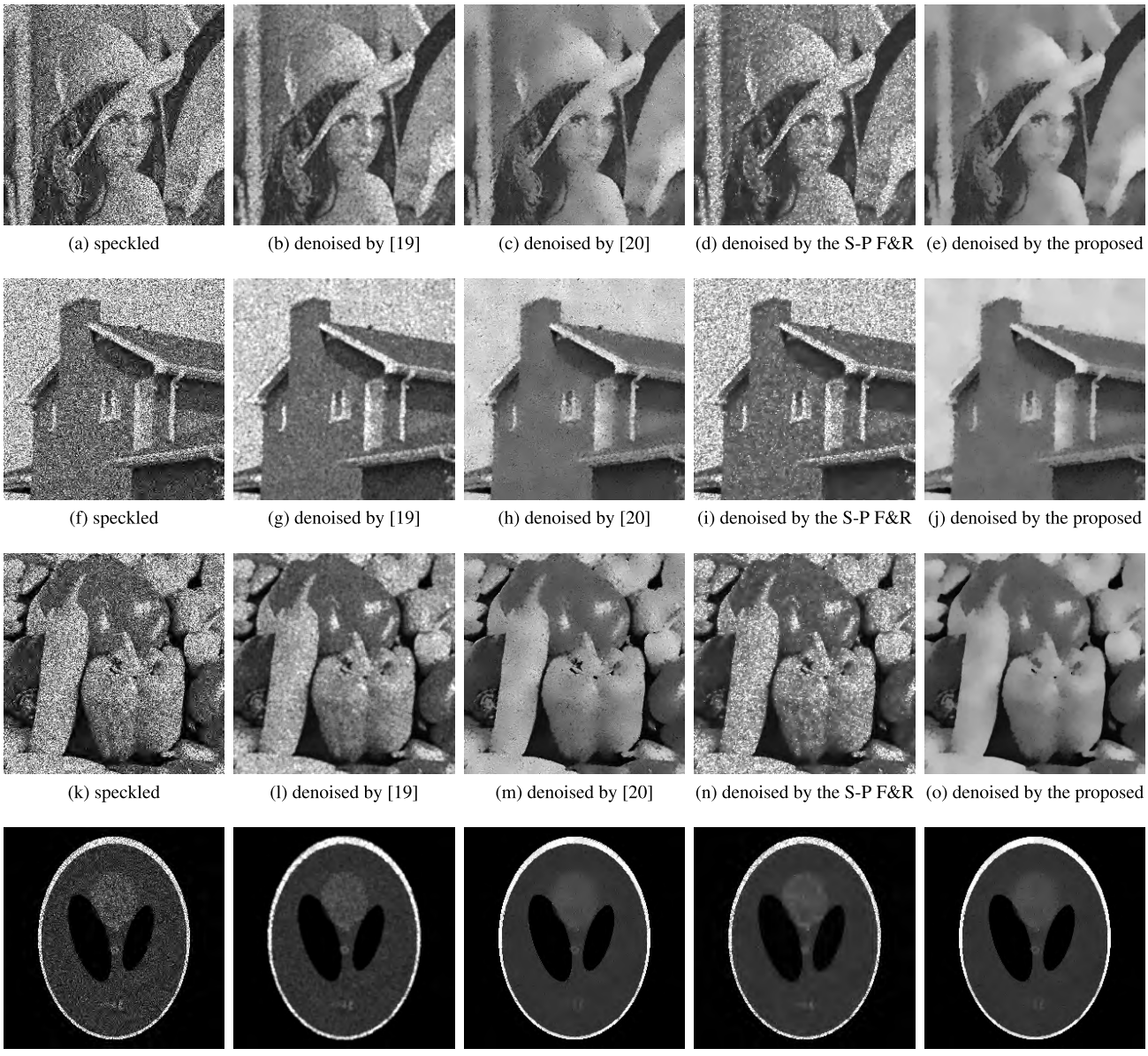

(a) speckled (b) denoised by [19] (c) denoised by [20] (d) denoised by the S-P F&R (e) denoised by the proposed

(f) speckled (g) denoised by [19] (h) denoised by [20] (i) denoised by the S-P F&R (j) denoised by the proposed

(k) speckled (l) denoised by [19] (m) denoised by [20] (n) denoised by the S-P F&R (o) denoised by the proposed

(p) speckled (q) denoised by [19] (r) denoised by [20] (s) denoised by the S-P F&R (t) denoised by the proposed

FIGURE 3. Speckled and denoised images for the Gamma distributed signal model ($P = 4$): (a)-(e): Lena, (f)-(j): House, (k)-(o): Peppers, and (p)-(t): "Shepp-Logan" phantom.

TABLE 3. SE between $\hat{\mathbf{u}}_{NLF}(\tilde{\theta})$ and $\mathbf{z}$ versus $\tilde{\theta}$ for OCT image.

$\tilde{\theta}$	0.5	0.6	0.7	0.8	0.9	1.0	1.1	1.2	1.3	1.4	1.5
$SE\ (dB)$	45.01	40.05	36.70	37.81	40.14	41.98	43.34	44.37	45.17	45.81	46.34

the OCT image as done in [49] and [50]. These metrics are defined based on the regions of interest (ROI) encompassing the high signal (media) part and the low signal (adventitia) part versus the noise background, which are depicted in Fig. 4. The signal-to-noise ratio (SNR) is defined as $SNR = 20\log_{10}(x_{lin}/\xi_{lin})$, where x_{lin} is the maximum intensity in the signal region, and ξ_{lin} is the standard deviation of the noise region, both in the linear scale. The contrast-to-noise ratio (CNR) is defined as $CNR = 20\log_{10}\left((\mu_x - \mu_b)/(\xi_x^2 - \xi_b^2)^{0.5}\right)$, where μ and ξ are the mean and standard deviation with the subscripts x and b denoting the signal and noise regions, respectively. The equivalent number of looks (ENL) is defined as $ENL = \mu_x^2/\xi_x^2$, and is averaged among the three blue ROIs depicted in Fig. 4. The definition of edge preservation factor (EPF) is shown at the bottom of the next page: where $x(i,j)$ and $\hat{x}(i,j)$ stand for the (i,j)-th pixel values of the original and denoised images, respectively, with Δ being the Laplace operator; $\Delta\bar{x}_r$ and $\Delta\bar{\hat{x}}_r$ stand for the mean values of $\Delta x(i,j)$ and $\Delta\hat{x}(i,j)$ in the r-th blue ROI, respectively. Here, $R = 3$. References [49] and [50]

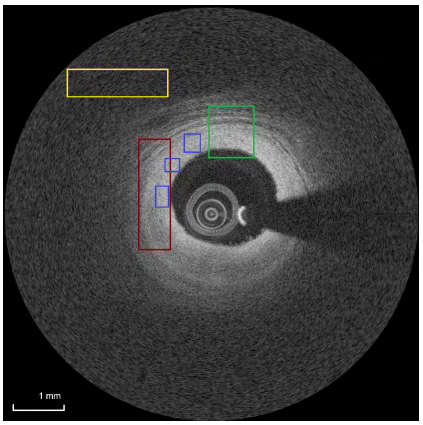

FIGURE 4. Original porcine carotid artery OCT image (Input SNR = 23.22 *dB*). The red ROI indicates the signal region and the yellow ROI indicates the noise region used in the metric calculation. The green ROI indicates the zoomed region in Fig. 6. The three blue ROIs are used for the ENL calculation.

provide the explanation of all these image quality metrics.

The corresponding denoised image by the proposed method together with those by [16], [20], [49] are shown in Fig. 5. For [16], we firstly apply the k-means clustering to the original OCT image. Then, disabling the effect from the other clusters, we utilize the Lee filter to enhance the central pixel of each sliding window.

For [49], the denoised image is obtained from

$$\begin{aligned}\hat{\mathbf{u}} &= \arg\min_{\mathbf{u}} f_r(\mathbf{u}) \\ &= \arg\min_{\mathbf{u}} \|\mathbf{z}-\mathbf{u}\|_2^2 + \lambda \sum_i \frac{1}{\beta(\beta-1)} \\ &\quad \cdot \left[u_i^{2\beta} + (\beta-1)s_i^{2\beta} - \beta u_i^2 \cdot s_i^{2(\beta-1)}\right], \end{aligned} \tag{39}$$

where β and λ are the user parameters tuning the performance of [49]; s_i is a reference image. Since the problem of (39) is decoupled, $\hat{\mathbf{u}}$ of (39) is solved iteratively as:

$$\mathbf{u}_{(k+1)} = \mathbf{u}_{(k)} - f_r'(\tilde{\mathbf{u}})|_{\tilde{\mathbf{u}}=\mathbf{u}_{(k)}} \Big/ f_r''(\tilde{\mathbf{u}})|_{\tilde{\mathbf{u}}=\mathbf{u}_{(k)}}, \tag{40}$$

for $k = 1, 2, \cdots$, with $f'(\cdot)$ and $f''(\cdot)$ denoting the first and second order derivative operators, respectively, and the initial value taken as s_i. For fairness, to implement the method [49], the denoised image produced by [20], is adopted as both the reference image and the initial value.

From Fig. 5, it is seen that [49] with a large β has nearly no impact on the observed image; while the proposed method provides higher SNR than [49] with a small β and [16], [20] within the similar EPF. Fig. 6 shows the enlarged views of the green region of the original and denoised OCT images, which is far from the catheter. By comparing the red ROI of Fig. 6 (b) with the corresponding parts of Figs. 6 (c)-(e), it is seen that the proposed method performs better in the speckle suppression. The above results demonstrate that our algorithm can better delineate features.

Table 4 lists more metric results of the above methods. From Table 4, it also demonstrates that [49] with a large β has tiny impact on the observed image. Besides, the proposed method provides the best results of SNR and ENL within the similar CNR and edge preservation. Based on the observation from Figs. 5, 6 and Table 4, it is reasonable to claim that the proposed method bear superior performance to the other compared methods. Note that a higher EPF will lower down the SNR performance of every denoising method.

TABLE 4. Metric comparison among original and denoised OCT images.

	SNR (dB)	CNR (dB)	ENL	EPF
Orignal	23.22	10.79	86.38	N/A
Proposed	28.06	11.47	661.70	0.0968
[16]	26.80	11.49	494.36	0.0946
[20]	27.15	11.51	449.63	0.0865
[49] ($\beta = 1.5,\ \lambda = 120$)	27.10	11.51	448.75	0.1399
[49] ($\beta = 4.0,\ \lambda = 1$)	22.71	10.99	102.95	0.9976

V. DISCUSSION

In this paper, we have proposed a general framework of the nonolocal means filtering to perform speckle removal, which is derived from the MAP estimation. The objective function of the corresponding optimization problem consists of two parts: the pixel fitting and total variation regularization terms. To avoid the step size selection in solving this optimization problem and make the computation tractable, the alternating direction method of multipliers is imposed, where the variables in the pixel fitting and regularization terms are split and optimized alternatively. The performance superiority of the proposed method in terms of various metrics is validated through the simulation on different speckle-corrupted synthetic images and the experiment on the real OCT image.

In addition, it should be pointed out that, in this paper, a generalized framework is proposed for despeckling. This means that the proposed method is not applicable only to one specific speckle model, but also to other kinds. Of course, since the noiseless image patch is not available in reality, the patch similarity measure in [20] is adopted as a substitute for the probability density function of the patch observation during the speckle removal. To design a similarity measure approximating the probability density function better is still one of the potential works.

In the future, we will go on with this topic, and address the issues of the reduction of the algorithm complexity,

$$EPF = 1/R\left(\sum_{r=1}^{R} \frac{\sum_{(i,j)\in r}(\Delta x(i,j)-\Delta\bar{x}_r)(\Delta\hat{x}(i,j)-\Delta\bar{\hat{x}}_r)}{\sqrt{\sum_{(i,j)\in r}(\Delta x(i,j)-\Delta\bar{x}_r)^2 \cdot \sum_{(i,j)\in r}(\Delta\hat{x}(i,j)-\Delta\bar{\hat{x}}_r)^2}}\right), \tag{38}$$

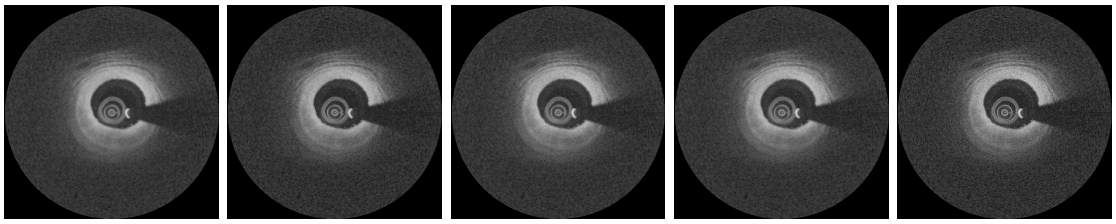

(a) (b) (c) (d) (e)

FIGURE 5. Denoised porcine carotid artery OCT images: (a) by the proposed algorithm (SNR = 28.06 *dB*), (b) by [16] (SNR = 26.80 *dB*), (c) by [20] (SNR = 27.15 *dB*), (d) by [49] (with $\beta = 1.5$, $\lambda = 120$. SNR = 27.10 *dB*), (e) by [49] (with $\beta = 4.0$, $\lambda = 1$. SNR = 22.71 *dB*).

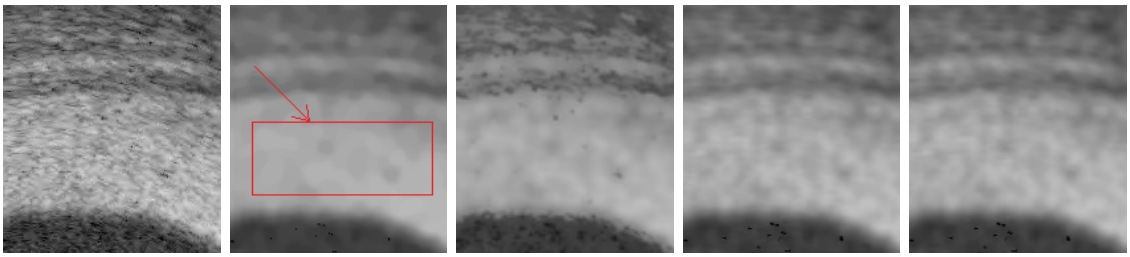

(a) (b) (c) (d) (e)

FIGURE 6. Enlarged view of the green region of the OCT images: (a) original, (b) denoised by the proposed algorithm, (c) denoised by [16], (d) denoised by [20], (e) denoised by [49] (with $\beta = 1.5$, $\lambda = 120$).

the selection of the size and shape of the patch in spatial filtering, and the nonlocal means filtering in the logarithmic scale and transform domains, which helps improve the despeckling performance promisingly.

ACKNOWLEDGMENT

The authors would like to gratefully appreciate the anonymous reviewers for their constructive remarks, which have notably improved the quality of this paper.

REFERENCES

[1] S. Sheela, M. Sumathi, and G. N. Priya, "Comparative analysis of various filtering techniques for speckle noise suppression in ultrasound images," *Int. J. Comput. Technol. Appl.*, vol. 9, no. 2, pp. 51–65, 2016.

[2] C. P. Loizou, C. S. Pattichis, C. I. Christodoulou, R. S. H. Istepanian, M. Pantziaris, and A. Nicolaides, "Comparative evaluation of despeckle filtering in ultrasound imaging of the carotid artery," *IEEE Trans. Ultrason., Ferroelectr., Freq. Control*, vol. 52, no. 10, pp. 1653–1669, Oct. 2005.

[3] A. C. Völker, P. Zakharov, B. Weber, F. Buck, and F. Scheffold, "Laser speckle imaging with an active noise reduction scheme," *Opt. Express*, vol. 13, no. 24, pp. 9782–9787, Nov. 2005.

[4] C. Oliver and S. Quegan, *Understanding Synthetic Aperture Radar Images*. Boston, MA, USA: Artech House, 1998.

[5] N. Yahya, N. S. Kamel, and A. S. Malik, "Subspace-based technique for speckle noise reduction in SAR images," *IEEE Trans. Geosci. Remote Sens.*, vol. 52, no. 10, pp. 6257–6271, Oct. 2014.

[6] F. Argenti, T. Bianchi, A. Lapini, and L. Alparone, "Fast MAP despeckling based on Laplacian–Gaussian modeling of wavelet coefficients," *IEEE Geosci. Remote Sens. Lett.*, vol. 9, no. 1, pp. 13–17, Jan. 2012.

[7] G. Andria, F. Attivissimo, A. M. L. Lanzolla, and M. Savino, "A suitable threshold for speckle reduction in ultrasound images," *IEEE Trans. Instrum. Meas.*, vol. 62, no. 8, pp. 2270–2279, Aug. 2013.

[8] H.-C. Li, W. Hong, Y.-R. Wu, and P.-Z. Fan, "Bayesian wavelet shrinkage with heterogeneity-adaptive threshold for SAR image despeckling based on generalized gamma distribution," *IEEE Trans. Geosci. Remote Sens.*, vol. 51, no. 4, pp. 2388–2402, Apr. 2013.

[9] F. Gao, X. Xue, J. Sun, J. Wang, and Y. Zhang, "A SAR image despeckling method based on two-dimensional S transform shrinkage," *IEEE Trans. Geosci. Remote Sens.*, vol. 54, no. 5, pp. 3025–3034, May 2016.

[10] H. Choi and J. Jeong, "Despeckling images using a preprocessing filter and discrete wavelet transform-based noise reduction techniques," *IEEE Sensors J.*, vol. 18, no. 8, pp. 3131–3139, Apr. 2018.

[11] V. S. Frost, J. A. Stiles, K. S. Shanmugan, and J. C. Holtzman, "A model for radar images and its application to adaptive digital filtering of multiplicative noise," *IEEE Trans. Pattern Anal. Mach. Intell.*, vol. PAMI-4, no. 2, pp. 157–166, Mar. 1982.

[12] D. T. Kuan, A. A. Sawchuk, T. C. Strand, and P. Chavel, "Adaptive noise smoothing filter for images with signal-dependent noise," *IEEE Trans. Pattern Anal. Mach. Intell.*, vol. PAMI-7, no. 2, pp. 165–177, Feb. 1985.

[13] J.-S. Lee, "Speckle suppression and analysis for synthetic aperture radar images," *Opt. Eng.*, vol. 25, no. 5, May 1986, Art. no. 255636.

[14] A. Buades, B. Coll, and J.-M. Morel, "A non-local algorithm for image denoising," in *Proc. IEEE Comput. Soc. Conf. Comput. Vis. Pattern Recognit.*, vol. 2. San Diego, CA, USA, Jun. 2005, pp. 60–65.

[15] S. Adabi, E. Rashedi, S. Conforto, D. Mehregan, Q. Xu, and M. Nasiriavanaki, "Speckle reduction of OCT images using an adaptive cluster-based filtering," in *Proc. SPIE Opt. Coherence Tomogr. Coherence Domain Opt. Methods Biomed. XXI*, San Francisco, CA, USA, vol. 10053, Feb. 2017, pp. 100532X-1–100532X-6.

[16] M. H. Eybposh, Z. Turani, D. Mehregan, and M. Nasiriavanaki, "Cluster-based filtering framework for speckle reduction in OCT images," *Biomed. Opt. Exp.*, vol. 9, no. 12, pp. 6359–6373, Dec. 2018.

[17] G. Chierchia, D. Cozzolino, G. Poggi, and L. Verdoliva, "SAR image despeckling through convolutional neural networks," in *Proc. IEEE Int. Geosci. Remote Sens. Symp.*, Jul. 2017, pp. 5438–5441.

[18] P. Wang, H. Zhang, and V. M. Patel, "SAR image despeckling using a convolutional neural network," *IEEE Signal Process. Lett.*, vol. 24, no. 12, pp. 1763–1767, Dec. 2017.

[19] Y. Guo, Y. Wang, and T. Hou, "Speckle filtering of ultrasonic images using a modified non local-based algorithm," *Biomed. Signal Process. Control*, vol. 6, no. 2, pp. 129–138, Apr. 2011.

[20] T. Teuber and A. Lang, "A new similarity measure for nonlocal filtering in the presence of multiplicative noise," *Comput. Statist. Data Anal.*, vol. 56, no. 12, pp. 3821–3842, 2012.

[21] Y. Zhan, M. Ding, L. Wu, and X. Zhang, "Nonlocal means method using weight refining for despeckling of ultrasound images," *Signal Process.*, vol. 103, pp. 201–213, Oct. 2014.

[22] S. M. Kay, *Fundamentals of Statistical Signal Processing: Estimation Theory*. Englewood Cliffs, NJ, USA: Prentice-Hall, 1993.

[23] L. I. Rudin, S. Osher, and E. Fatemi, "Nonlinear total variation based noise removal algorithms," *Phys. D, Nonlinear Phenomena*, vol. 60, nos. 1–4, pp. 259–268, 1992.

[24] S. D. Babacan, R. Molina, and A. K. Katsaggelos, "Variational Bayesian blind deconvolution using a total variation prior," *IEEE Trans. Image Process.*, vol. 18, no. 1, pp. 12–26, Jan. 2009.
[25] H. Madero-Orozco, P. Ruiz, J. Mateos, R. Molina, and A. K. Katsaggelos, "Image deblurring combining poisson singular integral and total variation prior models," in *Proc. 21st Eur. Signal Process. Conf.*, Marrakech, Morocco, Sep. 2013, pp. 1–5.
[26] C. Sutour, C.-A. Deledalle, and J.-F. Aujol, "Adaptive regularization of the NL-means: Application to image and video denoising," *IEEE Trans. Image Process.*, vol. 23, no. 8, pp. 3506–3521, Aug. 2014.
[27] S. P. Boyd and L. Vandenberghe, *Convex Optimization*. Cambridge, U.K.: Cambridge Univ. Press, 2004.
[28] D. P. Palomar and Y. C. Eldar, Eds., *Convex Optimization in Signal Processing and Communications*. Cambridge, U.K.: Cambridge Univ. Press, 2010.
[29] D. Gabay and B. Mercier, "A dual algorithm for the solution of nonlinear variational problems via finite element approximation," *Comput. Optim. Appl.*, vol. 2, no. 1, pp. 17–40, 1976.
[30] J. Eckstein and D. Bertsekas, "On the Douglas-Rachford splitting method and the proximal point algorithm for maximal monotone operators," *Math. Program.*, vol. 55, no. 3, pp. 293–318, Jun. 1992.
[31] D.-Q. Chen and L.-Z. Cheng, "Spatially adapted total variation model to remove multiplicative noise," *IEEE Trans. Image Process.*, vol. 21, no. 4, pp. 1650–1662, Apr. 2012.
[32] Y. Zhao, J. G. Liu, B. Zhang, W. Hong, and Y. R. Wu, "Adaptive total variation regularization based SAR image despeckling and despeckling evaluation index," *IEEE Trans. Geosci. Remote Sens.*, vol. 53, no. 5, pp. 2765–2774, May 2015.
[33] H. Woo and J. Ha, "Besta-divergence-based variational model for speckle reduction," *IEEE Signal Process. Lett.*, vol. 23, no. 11, pp. 1557–1561, Nov. 2016.
[34] G. Liu, H. Zhong, and L. Jiao, "Comparing noisy patches for image denoising: A double noise similarity model," *IEEE Trans. Image Process.*, vol. 24, no. 3, pp. 862–872, Mar. 2015.
[35] C. F. J. Wu, "On the convergence properties of the EM algorithm," *Ann. Statist.*, vol. 11, no. 1, pp. 95–103, Mar. 1983.
[36] J. M. Bioucas-Dias, M. A. T. Figueiredo, and J. P. Oliveira, "Total variation-based image deconvolution: A majorization-minimization approach," in *Proc. IEEE Int. Conf. Acoust., Speech Signal Process.*, Toulouse, France, vol. 2, Jul. 2006, pp. 861–864.
[37] J. Nocedal and S. J. Wright, *Numerical Optimization*. New York, NY, USA: Springer, 2006.
[38] M. V. Afonso, J. M. Bioucas-Dias, and M. A. T. Figueiredo, "An augmented Lagrangian approach to the constrained optimization formulation of imaging inverse problems," *IEEE Trans. Image Process.*, vol. 20, no. 3, pp. 681–695, Mar. 2011.
[39] J. W. Goodman, *Speckle Phenomena in Optics: Theory and Applications*. Englewood, CO, USA: Roberts, 2006.
[40] T. Eltoft, "Modeling the amplitude statistics of ultrasonic images," *IEEE Trans. Med. Imag.*, vol. 25, no. 2, pp. 229–240, Feb. 2006.
[41] J. C. Seabra and J. M. Sanches, "On estimating de-speckled and speckle components from B-mode ultrasound images," in *Proc. IEEE Int. Symp. Biomed. Imag., Nano Macro*, Rotterdam, The Netherlands, Apr. 2010, pp. 284–287.
[42] D. Koundal, S. Gupta, and S. Singh, "Speckle reduction method for thyroid ultrasound images in neutrosophic domain," *IET Image Process.*, vol. 10, no. 2, pp. 167–175, Feb. 2016.
[43] M. Pircher, E. Götzinger, R. Leitgeb, A. F. Fercher, and C. K. Hitzenberger, "Speckle reduction in optical coherence tomography by frequency compounding," *J. Biomed. Opt.*, vol. 8, no. 3, pp. 565–569, Jul. 2003.
[44] B. Karamata, K. Hassler, M. Laubscher, and T. Lasser, "Speckle statistics in optical coherence tomography," *J. Opt. Soc. Amer. A, Opt. Image Sci.*, vol. 22, no. 4, pp. 593–596, Apr. 2005.
[45] Q. Zhang, Y. Wu, W. Zhao, F. Wang, J. Fan, and M. Li, "Multiple-scale salient-region detection of SAR image based on gamma distribution and local intensity variation," *IEEE Geosci. Remote Sens. Lett.*, vol. 11, no. 8, pp. 1370–1374, Aug. 2014.
[46] M. Liu, Y. Wu, Q. Zhang, F. Wang, and M. Li, "Synthetic aperture radar target configuration recognition using locality-preserving property and the Gamma distribution," *IET Radar, Sonar Navigat.*, vol. 10, no. 2, pp. 256–263, 2016.
[47] L. A. Shepp and B. F. Logan, "The Fourier reconstruction of a head section," *IEEE Trans. Nucl. Sci.*, vol. NS-21, no. 3, pp. 21–43, Jun. 1974.
[48] J. Li, S. Liu, and E. Y. Lam, "Efficient source and mask optimization with augmented Lagrangian methods in optical lithography," *Opt. Express*, vol. 21, no. 7, pp. 8076–8090, Apr. 2013.
[49] K. H. Y. Cheng, E. Y. Lam, B. A. Standish, and V. X. D. Yang, "Speckle reduction of endovascular optical coherence tomography using a generalized divergence measure," *Opt. Lett.*, vol. 37, no. 14, pp. 2871–2873, Jul. 2012.
[50] P. Puvanathasan and K. Bizheva, "Speckle noise reduction algorithm for optical coherence tomography based on interval type II fuzzy set," *Opt. Exp.*, vol. 15, no. 24, pp. 15747–15758, Nov. 2007.

ZHENHUA ZHOU was born in Shanghai, China, in 1985. He received the bachelor's degree from the University of Shanghai for Science and Technology, in 2007, the master's degree from Shanghai Jiao Tong University. in 2010, and the Ph.D. degree from the City University of Hong Kong in 2013, all in electronic engineering.

He was a Research Associate with The Hong Kong University of Science and Technology, from 2016 to 2017. He is currently a Research Fellow with the College of Information Engineering, Shenzhen University. His research interests include spectral analysis, optimization, statistical signal processing, machine learning and their application to image processing, speech, and audio signal processing, and radar signal processing.

EDMUND Y. LAM (M'00–SM'05–F'15) received the B.S., M.S., and Ph.D. degrees in electrical engineering from Stanford University, Stanford, CA, USA, where he conducted research for the Programmable Digital Camera Project at the Information Systems Laboratory.

He has consulted for industry in the areas of digital camera systems design and algorithm development. From 2010 to 2011, he was invited to teach at the Department of Electrical Engineering and Computer Science, Massachusetts Institute of Technology, Cambridge, CA, USA, as a Visiting Associate Professor. He is currently a Professor of electrical and electronic engineering and an Associate Dean of Engineering (Teaching and Learning), as well as the Director of the Computer Engineering Program and the Founding Director of the Imaging Systems Laboratory, The University of Hong Kong. His current research interest includes computational imaging.

Dr. Lam is also a Fellow of the Optical Society (OSA), the Society of Photo-optical Instrumentation Engineers (SPIE), the Institute of Electrical and Electronics Engineers (IEEE), the Society for Imaging Science and Technology (IS&T), as well as the Hong Kong Institution of Engineers (HKIE). He was a recipient of the IBM Faculty Award.

CHUL LEE (S'06–M'13) received the B.S., M.S., and Ph.D. degrees in electrical engineering from Korea University, Seoul, South Korea, in 2003, 2008, and 2013, respectively.

He was with Biospace Inc., Seoul, from 2002 to 2006, where he was involved in the development of medical equipment. From 2013 to 2014, he was a Postdoctoral Scholar with the Department of Electrical Engineering, The Pennsylvania State University, University Park, PA, USA. From 2014 to 2015, he was a Research Scientist with the Department of Electrical and Electronic Engineering, The University of Hong Kong, Hong Kong. From 2015 to 2019, he was an Assistant Professor with the Department of Computer Engineering, Pukyong National University, Busan, South Korea. In March 2019, he joined the Department of Multimedia Engineering, Dongguk University, Seoul, where he is currently an Assistant Professor. His current research interests include image processing, and computational imaging with an emphasis on restoration and high dynamic range imaging.

Dr. Lee received the Best Paper Award from the *Journal of Visual Communication and Image Representation*, in 2014. He is also an Editorial Board Member of the *Journal of Visual Communication and Image Representation*.